ELSEVIER

Journal of Nuclear Materials 289 (2001) 177–187

journal of nuclear materials

www.elsevier.nl/locate/jnucmat

Heavy ion irradiation studies of columbite, brannerite, and pyrochlore structure types

Gregory R. Lumpkin *, Katherine L. Smith, Mark G. Blackford

Materials Division, Australian Nuclear Science and Technology Organisation, Private Mail Bag 1, Menai, NSW 2234, Australia

Abstract

Several natural and synthetic samples of pyrochlore, columbite, and brannerite were irradiated in situ in the high voltage electron microscope at Argonne National Laboratory using 1.5 MeV Kr^+ ions at room temperature. The columbite samples were selected because they have the same stoichiometry as brannerite and they exhibit a range of cation order prior to irradiation. The results of this study demonstrate that all the samples pass through the crystalline–amorphous transformation at a relatively low ion dose. For the AB_2O_6 oxides, D_c ranges from 0.8 to 1.5×10^{14} ions cm^{-2}, with little difference between the columbite and brannerite structure types. Within the group of columbite samples, there appears to be a systematic trend of increasing critical dose with increasing order parameter, although the critical doses are essentially within error of one another. Ordered columbites do not appear to revert to the subcell upon irradiation. The brannerite data set indicates a possible correlation between D_c and the mean atomic number of the A-site cation. The results for the two natural pyrochlores gave a slightly higher range of doses compared with the AB_2O_6 oxides. The pyrochlore data set indicates a possible correlation between D_c and the mean atomic number of the B-site cation. Electron diffraction results also suggest that the pyrochlore compositions irradiated in this work may not transform to the fluorite subcell until just before D_c is reached, if at all. For comparison, the samples investigated in this work have D_c values at room temperature that are generally on the low side of the range of values previously reported for synthetic zirconolite and pyrochlore samples ($2–6 \times 10^{14}$ ions cm^{-2}) under similar irradiation conditions.

PACS: 61.16.Bg; 61.50.Ks; 61.80.Jh

1. Introduction

Zirconolite and pyrochlore are well known as actinide host phases in titanate ceramics designed for the safe disposal of actinide-rich wastes, including weapons Pu [1–4]. More recently, brannerite has also been reported as a minor phase in these ceramics [5,6]. Due to the inherently high U content in brannerite (e.g., 62.8 wt% UO_2 in pure UTi_2O_6), there has been a considerable amount of interest in the crystal chemistry, radiation damage effects, and durability of this phase. In particular, studies of the crystal chemistry of synthetic brannerite have shown that considerable amounts of Ca and Gd can be incorporated in the structure with charge balance provided by U^{5+} ions [7]. Other studies have addressed the leaching behavior of metamict and annealed natural and synthetic brannerite, pyrochlore, and zirconolite over a range of pH values and temperature [8–10]. Initial results of these experiments suggest that brannerite may be the least durable of these phases in terms of uranium release. In parallel with the laboratory studies, recent work on natural brannerite has delineated the extent of incorporation of Ca, Y, lanthanides (Ln), Fe, Nb, and other elements, also suggesting that much of the U is present in a higher valence state than the normal U^{4+} state of the pure end-member. The natural samples have also provided evidence for alteration and U loss from brannerite in various geological environments (however, the total matrix durability is quite high) [11].

* Corresponding author. Tel.: +61-2 9717 3475; fax: +61-2 9543 7179.

E-mail address: grl@ansto.gov.au (G.R. Lumpkin).

0022-3115/01/$ - see front matter
PII: S0022-3115(00)00695-4

Another major concern for these structure types is that they will undergo a crystalline to amorphous transformation as a function of dose, which may lead to volume expansion, microfracturing, and reduced chemical durability. The radiation damage effects in zirconolite and pyrochlore have been studied extensively using heavy ion irradiation [12–15], actinide doping experiments [16–19], and natural samples [20–25], but little is known about the details of the transformation or the critical amorphization dose of brannerite. A recent work on the natural samples has confirmed that brannerite is rendered completely amorphous by alpha-decay processes, but the entire crystalline–amorphous transformation has not been observed primarily due to the high U content [11]. The main goal of this work is to examine the crystalline–amorphous transformation and determine the critical dose of several brannerite end-member compositions using ion irradiation techniques. In this work, we have used 1.5 MeV Kr^{+} ions in order to facilitate a comparison with previous work.

In order to assess the effect of structure type on the critical dose, we have also examined a small group of columbite and pyrochlore structure types. Although different from brannerite in detail, the structure of columbite is similar to brannerite in that both phases are AB_2O_6 oxides having two distinct octahedral sites in an array of oxygen atoms that are somewhat distorted from perfect hexagonal closest packing (HCP). The structure of pyrochlore, on the other hand, is quite different from the AB_2O_6 oxides and is one of the several derivatives of the fluorite structure type that are present in ceramic nuclear wasteforms. Heavy ion irradiation studies of these samples provide information that can be directly compared with their natural counterparts. These samples allow us to further investigate the transformation of superlattice structures to their respective subcells as a result of radiation damage. In particular, the columbite samples exhibit a range of cation order over two distinct octahedral sites *prior to irradiation*, from the completely disordered subcell through a partially ordered state to the fully ordered supercell. These samples provide a unique opportunity to determine the effect of the pre-existing cation distribution on the critical amorphization dose.

2. Experimental procedures

2.1. Sample description

Four of the columbites used in this study are natural samples with compositions close to $MnNbTaO_6$. All of these samples are from the Harding pegmatite, Taos County, NM. A previous work has shown that the Th and U contents of the samples are generally below 0.5 wt% and that the samples are highly crystalline, with diffraction patterns and microstructures characteristic of materials that have not reached the beginning of the crystalline–amorphous transformation [26]. These samples are therefore good candidates for irradiation work and do not require annealing before the irradiation experiments. We also examined a synthetic columbite having the composition $CaNb_2O_6$ that was prepared by sintering in air at 1300°C. Synthetic brannerites having compositions of $CeTi_2O_6$ and $ThTi_2O_6$ were prepared by sintering in air at 1400–1500°C, whereas UTi_2O_6 was prepared by hot pressing in a graphite die at 1200°C using 2 wt% Ti metal. In addition to these samples, two natural pyrochlores with compositions close to the ideal end-members $NaCaNb_2O_6F$ and $NaCaTa_2O_6F$ were examined. The $NaCaNb_2O_6F$ sample is from Russia and consisted of a large section of a pale brown single crystal from an alkaline igneous complex. The $NaCaTa_2O_6F$ sample is from Maine and consisted of several straw yellow crystals associated with albite, quartz, and tourmaline from the host granitic pegmatite.

2.2. Scanning electron microscopy (SEM)

All samples were checked for purity using a JEOL 6400 SEM operated at 15 kV. Inclusions, zoning, and other features were identified from a combination of secondary and backscattered electron images. Microanalyses were obtained using a Noran Voyager energy dispersive spectrometer (EDX) attached to this microscope. The instrument was calibrated for quantitative analysis using a range of synthetic and natural standard materials. Spectra were usually acquired for 500 s and reduced to weight percent oxides using a digital top hat filter to suppress the background, a library of reference spectra for multiple least-squares peak fitting, and full matrix corrections.

2.3. Transmission electron microscopy (TEM)

TEM samples were prepared by crushing small fragments in methanol and collecting the suspension on a copper grid with a holey carbon substrate. Basic sample characterization and detailed studies of cation ordering in the natural columbite samples were carried out using JEOL 2000FX and JEOL 2000FXII TEMs operated at 200 kV. Both instruments were calibrated for selected area diffraction work over a range of objective lens currents using a Au film standard. Cation ordering in columbite was investigated by taking selected area diffraction patterns in the [0 1 0] orientation using a double tilting specimen holder, 100 μm field limiting aperture, and a camera length of 83 cm (JEOL 2000FX). For this purpose, the illumination conditions and exposure times were carefully set up to give a constant current density for each crystal examined and to avoid saturation of the diffracted beams on the image

film. The compositions of the grains selected for irradiation were checked by EDX analysis using a Link ISIS EDX attached to the TEM (JEOL 2000FXII). The k-factors required for the quantitative thin film analyses were determined from a range of synthetic and natural standard materials. Spectra were usually acquired for 600 s and processed using a digital top hat filter to suppress the background, a library of reference spectra for multiple least-squares peak fitting, and a Cliff–Lorimer ratio procedure to reduce the data to weight percent oxides. The details of the TEM procedures are given in [27].

2.4. Heavy ion irradiation

Ion irradiation experiments were carried out in situ at the HVEM-Tandem User Facility at Argonne National Laboratory. TEM specimens were irradiated with 1.5 MeV Kr^+ ions at room temperature using a modified Kratos/AEI EM7 TEM interfaced to an NEC ion accelerator. All TEM observations were carried out using an operating voltage of 300 kV; however, the electron beam was always turned off during the irradiation steps in order to avoid unnecessary complications arising from simultaneous ion–electron interactions. A flux of 8.5×10^{11} ions cm^{-2} s^{-1} was used. The approximate sample temperature was monitored during the irradiations and never exceeded 35°C. To avoid the potential effects of ion channeling, grains were irradiated in random orientations. Each sample was irradiated incrementally and selected grains were observed using bright field imaging and selected area diffraction after each irradiation step. Using photographic negatives, the critical amorphization dose (D_c) was constrained to fall between the last dose increment in which Bragg diffraction spots were observed and the next increment in which only diffuse rings occur in the diffraction pattern. This is the appropriate procedure required to 'bracket' D_c when using an incremental irradiation technique or when the intensities of the Bragg diffracted beams cannot be recorded continuously as a function of dose [24,25]. For each phase, we determined D_c from the average of 3–6 grains (reported errors are one standard deviation on the mean value).

3. Structure and composition

3.1. Pyrochlore

Pyrochlore, conforming to the ideal general formula of $A_2B_2X_6Y$, is one of the several anion deficient derivatives of the fluorite structure type [28–30]. The structure of pyrochlore can be derived by removing one-eighth of the anions from the parent structure in an ordered manner, thereby reducing the coordination of half of the cation sites from eight to six and doubling the unit cell edge. The resulting space group is Fd3m (parent fluorite is Fm3m) and the only variable positional parameter is the x-coordinate of the X anions on 48f sites. A drawing of the structure is shown in Fig. 1. In the direct derivative structure, $x = 0.375$, the eight coordinated A-site remains a perfect cube, and the six coordinated B-site is a trigonally flattened octahedron. When $x = 0.4375$, the A-site becomes a trigonally flattened dodecahedron and the B-site is a perfect octahedron (see Fig. 1). In reality, in most natural and synthetic pyrochlores, the x-coordinate is close to 0.42 ± 0.01 [29]. Refinement of X-ray powder data for a sample of $NaCaTa_2O_6F$ from the Harding pegmatite gave $x = 0.43$ (G.R. Lumpkin, unpublished data). Bond lengths calculated from this value of x are B-$X = 0.1983$, A-$Y = 0.2258$, and A-$X = 0.2632$ nm.

In order to assess the potential effect of crystal structure on the critical amorphization doses of the three different structure types of this study, we have calculated the structural freedom (f) using Eq. (1) of Hobbs et al. [31]

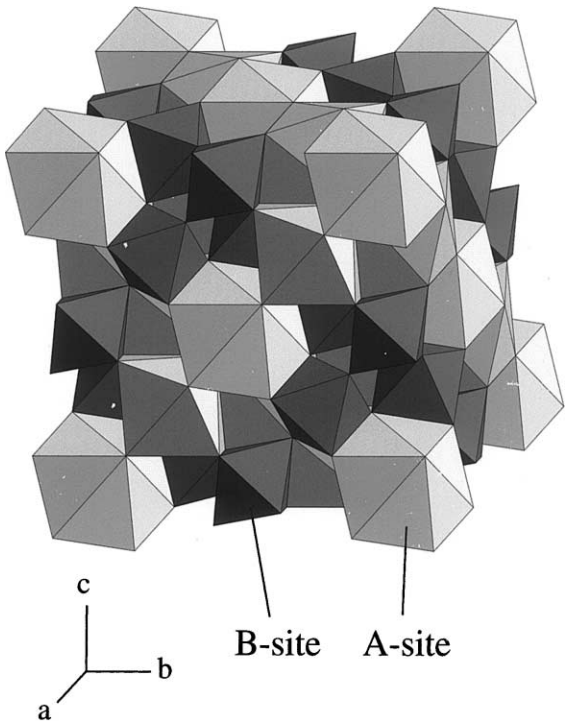

Fig. 1. Drawing of the crystal structure of pyrochlore, viewed down [3 1 1]. The X-anion coordinate (x) is 0.4375, for which the B-site is a perfect octahedron and the A-site is a trigonally flattened cube. Structure refinements indicate that x is near 0.42 for most pyrochlores. All anions are involved in edge-sharing, resulting in $f = -7.0$.

$$f = d - C\{\delta - [\delta(\delta+1)/2V]\} - (d-1)(Y/2) - [(p-1)d - (2p-3)](Z/p), \quad (1)$$

where V is the number of vertices in the polytope (e.g., TiO_6 octahedron or SiO_4 tetrahedron), C the average number of polytopes sharing each vertex, d the structure dimensionality, δ the dimensionality of the polytope, Y the fraction of edge-sharing vertices, and Z is the fraction of vertices sharing p-sided faces. For structures where $f < 0$, the structure is overconstrained and the material should be resistant to amorphization. When $f > 0$, the structure is underconstrained and '... extendable aperiodic arrangements can be propagated' [31]. In the pyrochlore structure, all anions are involved in edge-sharing, resulting in a calculated value of $f = -6.6$. For comparison, $f = -7.0$ for the parent fluorite structure type. However, the pyrochlore structure can also be viewed as two interpenetrating networks, one of which is a B_2X_6 octahedral framework and the other is an A_2Y tetrahedral framework (see Fig. 8 in ref. [30]). By considering only the B_2X_6 octahedral framework, often considered to be the fundamental structural unit of pyrochlore, calculation of the structural freedom gave $f = -1.0$. A separate calculation was performed for the A_2Y tetrahedral framework and yielded a value of $f = 0.0$.

As demonstrated in numerous previous investigations [32–36], the chemical composition of natural pyrochlore can be exceedingly complicated. For specimens having near ideal stoichiometry, the typical elements present on each site are A = Na, Ca, Sr, Ln, Th, and U; B = Nb, Ta, Ti, Zr, Sn, and W; X = O, and Y = O, OH, and F. Natural pyrochlores are characterized by extensive solid-solution, with substitution mechanisms ranging from simple Nb ↔ Ta substitution on the B-site to myriad coupled substitutions involving combinations of elements on the A-, B-, and Y-sites. For this study, we were fortunate to have at our disposal two natural samples having near end-member compositions of $NaCaNb_2O_6F$ and $NaCaTa_2O_6F$. SEM–EDX analyses showed that 4.3 wt% Nb_2O_5 is present as the only major impurity element in $NaCaTa_2O_6F$; 15 other elements, including Th and U, were processed and found to be near or below the detection limits of 0.1–0.3 wt%.

3.2. Columbite

The structure of columbite is a derivative of the alpha-PbO_2 structure type, in which the oxygen atoms assume HCP and the Pb atoms occupy one-half of the available octahedral interstices. In columbite [37,38], an AB_2O_6 oxide mineral of Mn, Fe, Nb, and Ta, the oxygen atoms are distorted somewhat from the ideal HCP configuration, the resulting symmetry is orthorhombic (space group Pbcn), and there are two distinct octahedral sites (4c and 8d). Typical bond lengths are 0.210–0.216 nm for the A-site and 0.185–0.214 nm for the B-site. The crystal structure of columbite is depicted in Fig. 2. Note in this drawing how the octahedra are linked by corner and edge-sharing to form a three-dimensional framework. The fundamental building units are zigzag chains of edge-sharing octahedra that run parallel to the c-axis. Individual chains are connected by corner-sharing, with each octahedral site sharing a total of two edges and four corners. For the columbite structure type, calculation of the structural freedom resulted in a value of $f = -4.0$. This value is a direct result of the fact that all the oxygen atoms are involved in edge-sharing.

X-ray and electron diffraction studies [26,39–42] indicate that the level of cation ordering in columbite varies in natural samples. In the disordered structure, the cations are randomly distributed over the octahedral sites at 4c and 8d, resulting in a unit cell with an a-cell dimension of approximately 0.48 nm. Ordering of Mn + Fe on 4c and Nb + Ta on 8d results in an ... ABBABB ... ordering sequence on (1 0 0) planes, resulting in a tripling of the a-axis to approximately 1.44 nm. Using electron diffraction, we determined that the fractional order parameters (q) of the four natural samples used in this study are approximately 0.0, 0.3, 0.6, and 1.0, where $q = 0.0$ for a disordered cation distribution and $q = 1.0$ for a fully ordered cation ar-

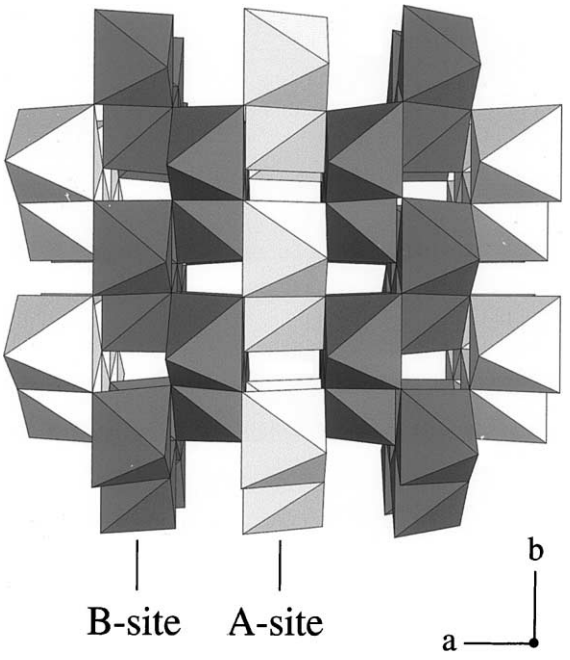

Fig. 2. Drawing of the crystal structure of columbite, viewed down [0 0 $\bar{1}$]. Note the ... ABBABB ... cation layers developed on (1 0 0) planes. All oxygens are involved in edge-sharing, resulting in $f = -4.0$.

rangement. Typical [0 1 0] zone axis electron diffraction patterns and intensity profiles taken along the (h02) reciprocal lattice rows are shown in Fig. 3, where the intensities of the superlattice reflections are directly proportional to the fractional order parameter.

The chemical composition of most natural columbite samples can be described by the four end-members $MnNb_2O_6$, $FeNb_2O_6$, $MnTa_2O_6$, and $FeTa_2O_6$. There is almost complete solid-solution between the four end-members in this system, with the exception of a small gap in compositions near $FeTa_2O_6$ [39,40]. In natural samples, Ti is often observed as a minor constituent, with lesser amounts of Sn and W reported in some examples. Other elements, including Y, Ln, and U are only rarely detected. SEM–EDX analyses show that all the four natural columbite samples used in this study are close to the intermediate composition $MnNbTaO_6$. On average, the analyses show that the samples contain less than 1 wt% TiO_2, less than 0.5 wt% FeO, and less than 0.2 wt% each of Y_2O_3, Ln_2O_3, WO_3, and UO_2. No significant elemental impurities were detected in the synthetic $CaNb_2O_6$ sample.

3.3. Brannerite

In the crystal structure of brannerite [43], a monoclinic (C2/m) uranium titanate ideally possessing AB_2O_6 stoichiometry, the oxygen atoms are also in a somewhat distorted HCP array, and half of the available octahedral sites are occupied. In pure end-member brannerite, the A-site (U) has bond lengths of 0.225–0.230 nm and the B-site (Ti) has bond lengths of 0.185–0.211 nm. As shown in Fig. 4, the structure consists of stepped layers of Ti octahedra connected by columns of U octahedra. The U octahedra are very regular in shape and form edge-sharing columns parallel to the *b*-axis, similar to the columns present in rutile. Each U octahedron

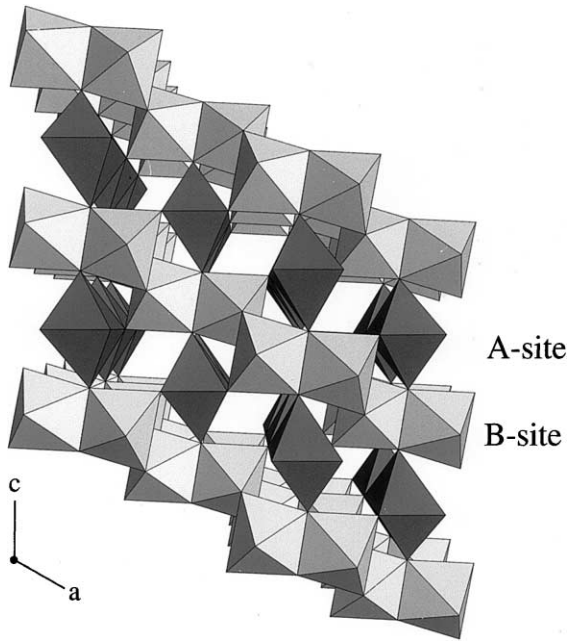

Fig. 4. Drawing of the crystal structure of brannerite, viewed down $[0\bar{1}0]$. Note how the structure consists of layers of Ti octahedra connected by edge-sharing columns of U octahedra. All oxygens are involved in edge-sharing, resulting in $f = -4.0$.

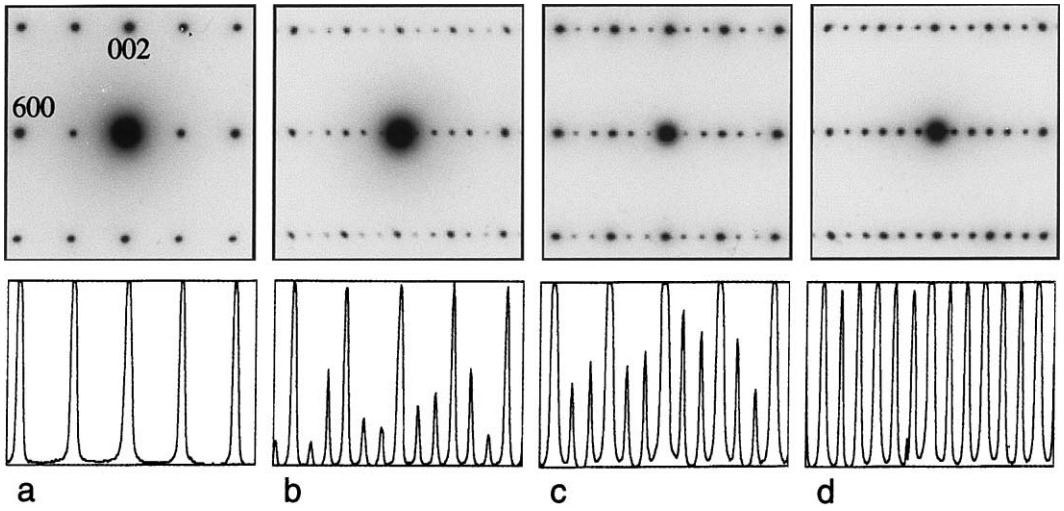

Fig. 3. Electron diffraction patterns and intensity profiles of the four natural columbite samples. All patterns are taken in the [0 1 0] zone axis orientation. (a) Highly disordered sample, $q = 0.0$. Note absence of superlattice spots along the (h0l) reciprocal lattice rows. (b) Partially ordered sample, $q = 0.3$. (c) Partially ordered sample, $q = 0.6$. (d) Highly ordered sample, $q = 1.0$. Note increasing intensity of superlattice spots from left to right.

shares two edges within the chain and four corners with Ti octahedra. The Ti octahedra in the stepped layers are distorted in a fashion similar to those in anatase. The basic building blocks within the stepped layers are zigzag chains of edge-sharing octahedra parallel to *b*-axis. Each Ti octahedron shares three edges with Ti octahedra and three corners with U octahedra. Calculation of the structural freedom for brannerite gave $f = -4.0$.

Recent investigations have shown that both synthetic [7] and natural brannerites [11] can incorporate substantial amounts of Ca, Y, Nb, Ln, Th, and other elements. The incorporation of lower valence elements on the A-site may be charge balanced by oxidation of some U^{4+} to U^{5+} and/or U^{6+} ions. SEM–EDX analyses of the synthetic UTi_2O_6 sample used in this study indicate that it is essentially stoichiometric, with no detectable impurities at the 0.1–0.3 wt% level. Therefore, considering the reducing conditions used for the preparation of the sample, the U in this sample is probably entirely in the 4+ valence state. No significant impurity elements were found in the $CeTi_2O_6$ and $ThTi_2O_6$ samples above detection limits. Because $CeTi_2O_6$ is very close to the ideal stoichiometry and was prepared in air, essentially all the Ce should be in the 4+ valence state.

4. Results

4.1. Pyrochlore

Results of the ion irradiation experiments are given in Table 1. As expected, both the pyrochlore samples were found to transform from the crystalline to the amorphous state. An example of the transformation is shown by the sequence of diffraction patterns for $NaCaTa_2O_6F$ in the top row of Fig. 5. The evolution of diffraction patterns with increasing ion dose is virtually identical to previous observations of synthetic pyrochlores doped with ^{238}Pu or ^{244}Cm [16,18,19] and natural pyrochlores containing ^{232}Th and ^{238}U [22,23]. The final, aperiodic structure is characterized by the presence of diffuse rings in the electron diffraction pattern with equivalent d-spacings of 0.30 and 0.18 nm. These values are virtually identical to those measured for natural samples that have been rendered completely amorphous by alpha-decay processes [22].

Similar observations were made for the $NaCaNb_2O_6F$ sample. Fig. 6 also shows that the (1 1 1) diffracted beams characteristic of the pyrochlore supercell are present up to the final stages of the transformation, before the material becomes fully amorphous. In this illustration, we have plotted a series of intensity profiles taken along a [1 1 1] reciprocal lattice row for one of the grains of $NaCaNb_2O_6F$ used in these experiments. Representing several dose increments, the profiles show that the (1 1 1) and (3 3 3) reflections characteristic of the pyrochlore superlattice are both present through the first half of the crystalline–amorphous transformation. The intensity of the (3 3 3) reflection diminishes rapidly at first, followed by the (1 1 1) reflection. However, both reflections persist through the latter half of the transformation, albeit with very low intensity.

We observed a significant difference in the critical amorphization doses of $NaCaNb_2O_6F$ and $NaCaTa_2O_6F$, with the two samples having average D_c values of 1.6×10^{14} and 2.5×10^{14} ions cm^{-2}, respectively. As indicated in Table 1, the only real difference between the two samples is the mean atomic number of the B-site cation (Z_B). Otherwise, the two samples have nearly identical amounts of Na, Ca, O, and F calculated on the basis of 2.00 B-site cations (the standard normalization scheme for pyrochlore [22,35,36]). Even the unit cell parameters are virtually identical at 1.043 nm. If valid, the observed difference in D_c suggests that heavier atoms on the B-site may promote a small increase in the critical amorphization dose at room temperature.

Table 1
Critical amorphization doses of columbite, brannerite, and pyrochlore after irradiation with 1.5 MeV Kr^+ ions at room temperature[a]

Sample	Structure type	Z_A	Z_B	q	D_c (10^{14} ions cm^{-2})
$MnNbTaO_6$	Columbite	25.0	57.0	0.0	0.8 ± 0.2
$MnNbTaO_6$	Columbite	25.0	57.0	0.3	1.0 ± 0.2
$MnNbTaO_6$	Columbite	25.0	57.0	0.6	1.2 ± 0.2
$MnNbTaO_6$	Columbite	25.0	57.0	1.0	1.5 ± 0.4
$CaNb_2O_6$	Columbite	20.0	41.0	1.0	1.4 ± 0.3
$CeTi_2O_6$	Brannerite	58.0	22.0	1.0	0.9 ± 0.1
$ThTi_2O_6$	Brannerite	90.0	22.0	1.0	1.2 ± 0.1
UTi_2O_6	Brannerite	92.0	22.0	1.0	1.5 ± 0.2
$NaCaNb_2O_6F$	Pyrochlore	15.5	41.0	1.0	1.6 ± 0.1
$NaCaTa_2O_6F$	Pyrochlore	15.5	73.0	1.0	2.5 ± 0.3

[a] Z_A and Z_B are the mean atomic numbers of the A- and B-sites. The parameter q gives the average level of cation order over these sites.

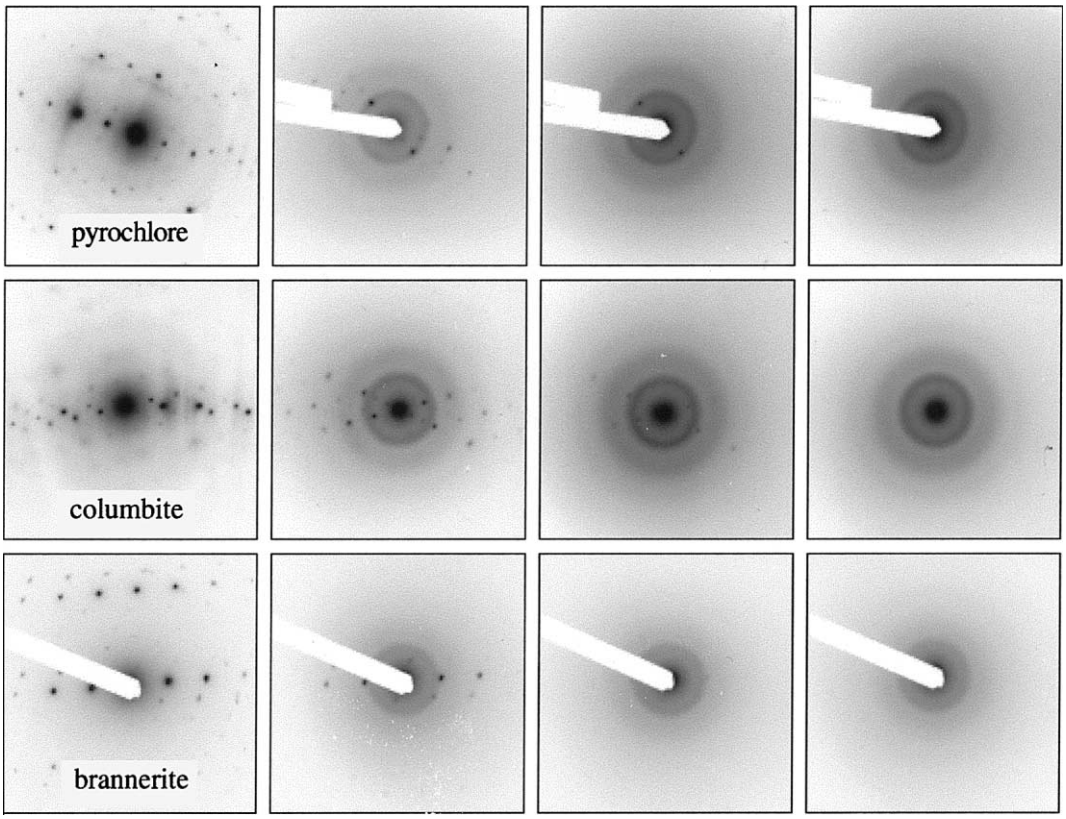

Fig. 5. Electron diffraction patterns of samples irradiated with 1.5 MeV Kr^+ ions at room temperature. Top row: $NaCaTa_2O_6F$ pyrochlore structure; unirradiated, 1.6×10^{14}, 2.4×10^{14}, 3.1×10^{14} ions cm^{-2} . Middle row: $CaNb_2O_6$ ordered columbite structure; unirradiated, 0.8×10^{14}, 1.2×10^{14}, 1.6×10^{14} ions cm^{-2}. Bottom row: $CeTi_2O_6$ brannerite structure; unirradiated, 0.4×10^{14}, 0.8×10^{14}, 1.0×10^{14} ions cm^{-2}.

4.2. Columbite

All four natural columbite samples and synthetic $CaNb_2O_6$, transformed to the amorphous state with increasing ion dose. The irradiation-induced transformation observed in these samples is generally consistent with previous work on natural U bearing columbite samples from Western Australia [44]. Diffraction patterns of all five samples follow the simple sequence described previously for natural pyrochlores [22]. The diffraction patterns exhibit a continuous change from the crystalline to the amorphous state as a function of ion irradiation dose, without the formation of highly tilted domains or subgrains observed in some silicate minerals (representative diffraction patterns are shown for $CaNb_2O_6$ in the middle row of Fig. 5). Intensity profiles were obtained from ordered columbite grains with favorable orientations and these showed that the superlattice reflections persist through most of the crystalline–amorphous transformation, similar to the pyrochlores investigated in this study. The final state of damage is characterized by the presence of diffuse rings with equivalent d-spacings of 0.31 and 0.18 nm.

The average D_c values of the four natural samples range from 0.8×10^{14} to 1.5×10^{14} ions cm^{-2}, but as indicated in Table 1 they are almost within error of one another. However, there is a systematic trend of increasing critical dose with increasing order parameter in the four $MnNbTaO_6$ natural samples and this appears to be confirmed by the D_c value of the fully ordered, synthetic $CaNb_2O_6$ sample (see Table 1). This trend indicates that samples with pre-existing cation order prior to irradiation with 1.5 MeV Kr^+ ions at room temperature are somewhat more difficult to amorphize than their partially ordered or disordered counterparts.

4.3. Brannerite

The three synthetic brannerite samples all reached the electron diffraction amorphous state at doses that are similar to the five columbite samples and one of the two pyrochlore samples examined in this study (Table 1). Amorphization of brannerite by heavy ion irradiation is

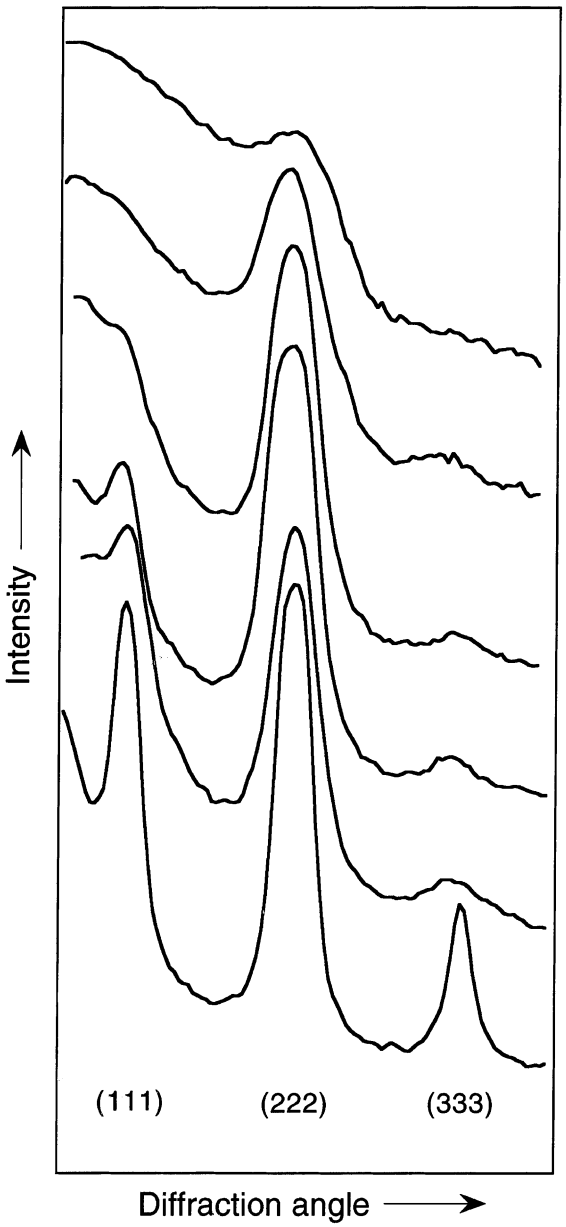

Fig. 6. Intensity profiles of $NaCaNb_2O_6F$ pyrochlore showing persistence of (1 1 1) and (3 3 3) superlattice spots up to the highest ion dose levels, just prior to complete amorphization. From bottom to top, dose levels are: unirradiated, 0.8×10^{14}, 1.0×10^{14}, 1.2×10^{14}, 1.4×10^{14}, 1.8×10^{14} ions cm^{-2}.

consistent with the observation of metamict (amorphous) brannerite in nature [11,45,46]. These samples also exhibit a simple, continuous crystalline–amorphous transformation with increasing ion dose, without the formation of highly tilted domains or subgrains. Furthermore, there are no intermediate phases that form during the transformation process (representative diffraction patterns are shown for $CeTi_2O_6$ in the bottom row of Fig. 5). Fully amorphous brannerite samples exhibit diffuse rings in their electron diffraction patterns with equivalent d-spacings of 0.30 and 0.19 nm.

D_c values of the synthetic brannerites range from 0.9×10^{14} to 1.5×10^{14} ions cm^{-2} and overlap almost exactly with the columbite samples. The critical amorphization dose results for each sample are listed in Table 1 and suggest that the critical dose increases systematically as a function of the mean atomic number of the A-site cation (Z_A) from $CeTi_2O_6$ to $ThTi_2O_6$ to UTi_2O_6. However, reported standard deviations show that the critical dose values of $ThTi_2O_6$ and UTi_2O_6 are essentially within error of one another (see Table 1), as expected from the similarity in atomic number of Th and U.

5. Discussion and conclusions

Results of this study demonstrate that all three of the Ti, Nb, and Ta oxide structure types pass through the crystalline–amorphous transformation at a relatively low ion dose. In detail, the transformation closely resembles the simple sequence observed by Lumpkin and coworkers in natural columbites, pyrochlores, and zirconolites [21–25,44]. The available data from actinide doping experiments conducted in the 1980's indicates that a similar model applies to the samples doped with short-lived ^{238}Pu or ^{244}Cm [16–19]. With increasing dose, these structure types amorphize by accumulation of isolated alpha-recoil collision cascades, overlap of cascades to produce larger amorphous domains, and continued growth of these domains until the materials no longer possess periodicity beyond the second coordination sphere (e.g., beyond the metal–metal distances) [21,47–51]. Amorphization by heavy ion irradiation is consistent with this model, with the caveat that damage is produced in electron transparent samples (e.g., approximately 50–200 nm thick) in the HVEM by subcascades of the primary ions as they pass through the crystal. The final damage state in the samples irradiated with 1.5 MeV Kr^+ ions appears to be similar to the natural and actinide doped samples, as evidenced by the presence of diffuse rings with equivalent d-spacings of approximately 0.30–0.31 and 0.18–0.19 nm in electron diffraction patterns. These values are nearly identical to those reported previously for natural samples [20–22,44].

For the AB_2O_6 oxides, D_c ranges from 0.8 to 1.5×10^{14} ions cm^{-2}, with little difference between the columbite and brannerite structure types. Although the structures differ in detail, the general features are very similar. Both columbite and brannerite are based on a somewhat distorted hexagonal closest packed array of oxygen atoms with two distinct octahedral sites. These sites are connected by a combination of edge- and cor-

ner-sharing to form three-dimensional framework structures. Furthermore, the two minerals have similar ranges of A–O and B–O bond lengths. Not surprisingly then, the calculated values of the structural freedom are identical ($f = -4.0$) for these two structure types, and are consistent with the ion irradiation results.

In comparison, the D_c values of the two pyrochlores irradiated in this work are generally higher than the AB_2O_6 oxides. This result is in qualitative agreement with the lower value of the structural freedom ($f = -6.6$) calculated for the whole structure (lower values of f are characteristic of materials with higher critical amorphization doses [31]). Consideration of the B_2O_6 framework alone ($f = -1.0$) is inconsistent with the results observed in this study. Smith et al. [52] have recently noted that the structural freedom parameter does not successfully predict the relative susceptibility to amorphization of freudenbergite, perovskite, and zirconolite when using specific structural elements (e.g., the Ti–O frameworks of freudenbergite and perovskite, the Ti–O layers of zirconolite). Although we believe that the concept of structural freedom as developed by Hobbs et al. [31] is useful, in practice it may be difficult to apply when dealing with complex structure types. The model does, in general, predict the behavior of a large group of materials under irradiation and could be incorporated as part of a more detailed radiation model. Wang and coworkers [53,54] have incorporated some of the concepts of structural freedom in a detailed, semi-empirical radiation damage model that successfully predicts the behavior of phases in the system $MgO–Al_2O_3–SiO_2$.

All of the samples investigated in this work have D_c values at room temperature that are generally on the low side of the range of values previously reported for synthetic zirconolite and pyrochlore samples irradiated with 1.0 or 1.5 MeV Kr^+ ions ($2–6 \times 10^{14}$ ions cm^{-2}) [12,14,15,55]. The previously studied pyrochlore compositions include $CaU(Ti,Zr)_2O_7$ and several $Ln_2Ti_2O_7$ end-members [14,15]. Why do the pyrochlore samples irradiated in this work have lower D_c values than those studied previously? One possible explanation is that the Na–F pyrochlores are inherently more susceptible to amorphization at room temperature due to lower displacement energies (E_d) of the cations. Unfortunately, at present there are no experimental data available to test this proposition. Another idea recently advanced from a study of freudenbergite is that mobility of alkali ions such as Na may present an additional complication during ion irradiation of thin specimens in the HVEM [52]. The available experimental data on complex silicates [56] appear to support this idea and it is well known that albite ($NaAlSi_3O_8$) loses Na prior to amorphization during electron irradiation in the TEM [57]. A third possibility recently advanced by Wang et al. [58] is that differences in the amorphization dose (and critical temperature) are related to the cation masses of the target material. In this model, samples with lower cation masses should produce higher D_c values under similar irradiation conditions. We note that this effect was not observed in a similar study by Begg et al. [59] and the opposite effect is indicated in the present study.

Within the group of columbite samples, there appears to be a systematic trend of increasing critical dose with increasing order parameter, although the critical doses are essentially within error of one another. These results indicate that, at best, there is only a minor increase in D_c associated with the level of pre-existing cation order. Furthermore, electron diffraction data presented in this paper indicate that the ordered columbite samples do not appear to revert to the subcell upon irradiation. Because the crystalline–amorphous transformation typically spans a dose range covering one order of magnitude or more from beginning to end, we would have expected a significant gain in D_c as a function of q for the four natural columbites and fully ordered $CaNb_2O_6$.

Electron diffraction results also suggest that the pyrochlore compositions irradiated in this study may not transform to the fluorite subcell until just before D_c is reached, if at all. These results bring into question the reported transformation to the fluorite subcell during the crystalline–amorphous transformation process [14,15,20,55]. The results of the present work are consistent with a previous work on natural pyrochlores from the Harding pegmatite, where the (1 1 1) and other superlattice reflections in X-ray and electron diffraction patterns persisted through most of the crystalline–amorphous transformation [22]. Weber et al. [19] have also published electron diffraction patterns of Cm doped $Gd_2Ti_2O_7$ in which the (1 1 1) superlattice spots are still present at a relatively high alpha-decay dose. Furthermore, the X-ray diffraction data of Wald et al. [16] indicate that the Cm doped zirconolite $CaZrTi_2O_7$ does not transform to fluorite during the crystalline–amorphous transformation. However, in the $Gd_2Ti_2O_7$–$Gd_2Zr_2O_7$ solid-solution series, it has been observed that the Zr-rich pyrochlores are highly resistant to amorphization and transform to a defect fluorite structure under irradiation [60,61]. These pyrochlores have the lowest ionic radius ratio values ($r_A/r_B < 1.52$, closest to fluorite) and also exhibit a high temperature transformation to a defect fluorite structure. In comparison, the pyrochlores irradiated in this study have $r_A/r_B = 1.80$ and, as far as we know, do not disorder to a defect fluorite phase at high temperature.

In conclusion, there is a clear need to resolve some of the outstanding issues concerning the amorphization of pyrochlores, especially the conflicting information on the effect of composition on the critical dose. Further detailed work on the crystal chemistry and phase relations should shed light on the radiation-induced transformation of pyrochlore to the defect fluorite structure as a function of composition.

Acknowledgements

We thank M. Colella, S.H.F. Leung, and R.A. Day for assistance with the SEM and TEM work and for general maintenance of the laboratories and equipment at Ansto. Lou Vance and Adam Jostsons provided helpful comments prior to submission of the manuscript. This work would not have been possible without assistance from Ed Ryan, Stan Ockers, and Tony McCormick of the HVEM-Tandem User Facility at Argonne. This facility is supported as a User Facility by the US-DOE, Basic Energy Sciences, under contract W-31-109-ENG-38.

References

[1] A.E. Ringwood, S.E. Kesson, K.D. Reeve, D.M. Levins, E.J. Ramm, in: W. Lutze, R.C. Ewing (Eds.), Radioactive Waste Forms for the Future, North-Holland, Amsterdam, 1988, p. 233.
[2] A.B. Harker, in: W. Lutze, R.C. Ewing (Eds.), Radioactive Waste Forms for the Future, North-Holland, Amsterdam, 1988, p. 335.
[3] P.E. Fielding, T.J. White, J. Mater. Res. 2 (1987) 387.
[4] E.R. Vance, Mater. Res. Soc. Bull. 19 (1994) 28.
[5] B.R. Myers, G.A. Armantrout, C.M. Jantzen, A. Jostsons, J.M. McKibben, H.F. Shaw, D.M. Strachan, J.D. Vienna, Technical Evaluation Panel Summary Report: Ceramic and Glass Immobilization Options, Plutonium Immobilization Project, UCRL-ID-129315, 1998.
[6] B.B. Ebbinghaus, R. Van Konynenburg, F.J. Ryerson, E.R. Vance, M.W.A. Stewart, A. Jostsons, J.S. Allender, T. Rankin, J. Congdon, Presented at Waste Management '98 (CD-ROM), Tucson, AZ, 1998.
[7] E.R. Vance, J.N. Watson, M.L. Carter, R.A. Day, G.R. Lumpkin, K.P. Hart, Y. Zhang, P.J. McGlinn, M.W.A. Stewart, D.J. Cassidy, Presented at the American Ceramic Society Annual Meeting, Indianapolis, IN, 1999.
[8] W. Bourcier, S.K. Roberts, H.F. Shaw, Presented at the Seventh International Conference on the Chemistry and Migration Behavior of Actinides and Fission Products in the Geosphere, Migration '99, Lake Tahoe, NV, 1999, Abstracts, p. 32.
[9] Y. Zhang, G.R. Lumpkin, K. Hart, R. Day, S. Leung, Z. Aly, M. Carter, Presented at the Seventh International Conference on the Chemistry and Migration Behavior of Actinides and Fission Products in the Geosphere, Migration '99, Lake Tahoe, NV, 1999, Abstracts, p. 18.
[10] A.J. Bakel, V.N. Zyryanov, C.J. Mertz, E.C. Buck, D.B. Chamberlain, in: D.J. Wronkiewicz, J.H. Lee (Eds.), Mater. Res. Soc. Symp. Proc. 556 (1999) 181.
[11] G.R. Lumpkin, M. Colella, S.H.F. Leung, in: R.W. Smith, D.W. Shoesmith (Eds.), Mater. Res. Soc. Symp. Proc. 608 (2000) 359.
[12] R.C. Ewing, L.M. Wang, Nucl. Instrum. and Meth. B 65 (1992) 319.
[13] W.J. Weber, N.J. Hess, G.D. Maupin, Nucl. Instrum. and Meth. B 65 (1992) 102.
[14] K.L. Smith, N.J. Zaluzec, G.R. Lumpkin, J. Nucl. Mater. 250 (1997) 36.
[15] S.X. Wang, L.M. Wang, R.C. Ewing, G.S. Was, G.R. Lumpkin, Nucl. Instrum. and Meth. B 148 (1999) 704.
[16] J.W. Wald, P. Offermann, in: W. Lutze (Ed.), Scientific Basis for Nuclear Waste Management V, Elsevier, New York, 1982, p. 369.
[17] F.W. Clinard Jr., D.L. Rohr, R.B. Roof, Nucl. Instrum. and Meth. B 1 (1984) 581.
[18] F.W. Clinard Jr., D.E. Peterson, D.L. Rohr, L.W. Hobbs, J. Nucl. Mater. 126 (1984) 245.
[19] W.J. Weber, J.W. Wald, H.J. Matzke, J. Nucl. Mater. 138 (1986) 196.
[20] R.C. Ewing, T.J. Headley, J. Nucl. Mater. 119 (1983) 102.
[21] G.R. Lumpkin, R.C. Ewing, B.C. Chakoumakos, R.B. Greegor, F.W. Lytle, E.M. Foltyn, F.W. Clinard Jr., L.A. Boatner, M.M. Abraham, J. Mater. Res. 1 (1986) 564.
[22] G.R. Lumpkin, R.C. Ewing, Phys. Chem. Minerals 16 (1988) 2.
[23] G.R. Lumpkin, K.P. Hart, P.J. McGlinn, T.E. Payne, R. Gieré, C.T. Williams, Radiochim. Acta 66&67 (1994) 469.
[24] G.R. Lumpkin, K.L. Smith, R. Gieré, Micron 28 (1997) 57.
[25] G.R. Lumpkin, K.L. Smith, M.G. Blackford, R. Gieré, C.T. Williams, in: I.G. McKinley, C. McCombie (Eds.), Mater. Res. Soc. Symp. Proc. 506 (1998) 215.
[26] G.R. Lumpkin, Can. Mineral. 36 (1998) 585.
[27] G.R. Lumpkin, K.L. Smith, M.G. Blackford, R. Gieré, C.T. Williams, Micron 25 (1994) 581.
[28] M.A. Subramanian, G. Aravamudan, G.V. Subba Rao, Prog. Solid State Chem. 15 (1983) 55.
[29] B.C. Chakoumakos, J. Solid State Chem. 53 (1984) 120.
[30] K.L. Smith, G.R. Lumpkin, in: J.N. Boland, J.D. Fitz Gerald (Eds.), Defects and Processes in the Solid State: Geoscience Applications, the McLaren Volume, Elsevier, Amsterdam, 1993, p. 401.
[31] L.W. Hobbs, A.N. Sreeram, C.E. Jesurum, B.A. Berger, Nucl. Instrum. and Meth. B 116 (1996) 18.
[32] D.D. Hogarth, Can. Mineral. 6 (1961) 610.
[33] G. Perrault, Can. Mineral. 9 (1968) 383.
[34] W. Petruk, D.R. Owens, Can. Mineral. 13 (1975) 282.
[35] D.D. Hogarth, Am. Mineral. 62 (1977) 403.
[36] G.R. Lumpkin, B.C. Chakoumakos, R.C. Ewing, Am. Mineral. 71 (1986) 569.
[37] J.R. Sturdivant, Z. Kristallogr. 75 (1930) 88.
[38] E.H. Nickel, J.F. Rowland, R.C. McAdam, Am. Mineral. 48 (1963) 961.
[39] P. Cerny, T.S. Ercit, Bull. Mineral. 108 (1985) 499.
[40] P. Cerny, T.S. Ercit, in: P. Möller, P. Cerny, F. Saupe (Eds.), Lanthanides, Tantalum and Niobium, Springer, Berlin, 1989, p. 27.
[41] M. Wenger, T. Armbruster, Schweiz. Mineral. Petrogr. Mitt. 71 (1991) 349.
[42] T.S. Ercit, M.A. Wise, P. Cerny, Am. Mineral. 80 (1995) 613.
[43] J.T. Szymanski, J.D. Scott, Can. Mineral. 20 (1982) 271.
[44] G.R. Lumpkin, J. Nucl. Mater. 190 (1992) 302.
[45] A. Pabst, Am. Mineral. 39 (1954) 109.
[46] F. Bianconi, A. Simonetti, Schweiz. Mineral. Petrogr. Mitt. 47 (1967) 887.
[47] R.B. Greegor, F.W. Lytle, B.C. Chakoumakos, G.R., Lumpkin, R.C. Ewing, in: C.M. Jantzen, J.A. Stone, R.C. Ewing (Eds.), Mater. Res. Soc. Symp. Proc. 44 (1985) 655.

[48] R.B. Greegor, F.W. Lytle, B.C. Chakoumakos, G.R., Lumpkin, R.C. Ewing, in: L.O. Werme (Ed.), Mater. Res. Soc. Symp. Proc. 50 (1986) 387.
[49] R.B. Greegor, F.W. Lytle, B.C. Chakoumakos, G.R., Lumpkin, R.C. Ewing, C.L. Spiro, J. Wong, in: J.K. Bates, W.B. Seefeldt (Eds.), Mater. Res. Soc. Symp. Proc. 84 (1987) 645.
[50] R.B. Greegor, F.W. Lytle, B.C. Chakoumakos, G.R., Lumpkin, J.K. Warner, R.C. Ewing, in: W. Lutze, R.C. Ewing (Eds.), Mater. Res. Soc. Symp. Proc. 127 (1989) 261.
[51] F. Farges, R.C. Ewing, G.E. Brown Jr., J. Mater. Res. 8 (1993) 1983.
[52] K.L. Smith, M.G. Blackford, G.R. Lumpkin, N.J. Zaluzec, J. Nucl. Mater. 277 (2000) 159.
[53] S.X. Wang, G.R. Lumpkin, L.M. Wang, R.C. Ewing, Nucl. Instrum. and Meth. B 166&167 (2000) 293.
[54] L.M. Wang, S.X. Wang, W.L. Gong, R.C. Ewing, in: I.M. Robertson, G.S. Was, L.W. Hobbs, T. Diaz de la Rubia (Eds.), Mater. Res. Soc. Symp. Proc. 439 (1997) 619.
[55] S.X. Wang, L.M. Wang, R.C. Ewing, in: I.M. Robertson, G.S. Was, L.W. Hobbs, T. Diaz de la Rubia (Eds.), Mater. Res. Soc. Symp. Proc. 439 (1997) 583.
[56] R.K. Eby, R.C. Ewing, R.C. Birtcher, J. Mater. Res. 7 (1992) 3080.
[57] I.D.R. Mackinnon, G.R. Lumpkin, S.B. Van Deusen, in: A.D. Romig Jr., W.F. Chambers (Eds.), Microbeam Analysis – 1986, San Francisco Press, San Francisco, 1986, p. 451.
[58] S.X. Wang, L.M. Wang, R.C. Ewing, K.V. Govindan Kutty, Nucl. Instrum. and Meth. B 169 (2000) 135.
[59] B.D. Begg, W.J. Weber, R. Devanathan, J.P. Icenhower, S. Thevuthasan, B.P. McGrail, Ceramic Trans. 107 (2000) 553.
[60] S.X. Wang, L.M. Wang, R.C. Ewing, K.V.G. Kutty, in: S.J. Zinkle, G.E. Lucas, R.C. Ewing, J.S. Williams (Eds.), Mater. Res. Soc. Symp. Proc. 540 (1999) 355.
[61] B.D. Begg, N.J. Hess, D.E. McCready, S. Thevuthasan, W.J. Weber, these Proceedings.